

Lyapunov Exponents for the Intermittent Transition to Chaos

James Hanssen^a and **Walter Wilcox^{a,b}**

^aDepartment of Physics, Baylor University, Waco, TX 76798

^bDepartment of Physics, University of Kentucky, Lexington, KY 40506

Abstract

The dependence of the Lyapunov exponent on the closeness parameter, ϵ , in tangent bifurcation systems is investigated. We study and illustrate two averaging procedures for defining Lyapunov exponents in such systems. First, we develop theoretical expressions for an isolated tangency channel in which the Lyapunov exponent is defined on single channel passes. Numerical simulations were done to compare theory to measurement across a range of ϵ values. Next, as an illustration of defining the Lyapunov exponent on many channel passes, a simulation of the intermittent transition in the logistic map is described. The modified theory for the channels is explained and a simple model for the gate entrance rates is constructed. An important correction due to the discrete nature of the iterative flow is identified and incorporated in an improved model. Realistic fits to the data were made for the Lyapunov exponents from the logistic gate and from the full simulation. A number of additional corrections which could improve the treatment of the gates are identified and briefly discussed.

1. Introduction and Background

Chaos is the study of dynamical systems that have a sensitive dependence on initial conditions. Much attention has been paid to the two main routes to chaos: pitchfork bifurcation and tangent bifurcation. If we consider the general difference equation mapping,

$$x_{n+1} = F(x_n), \quad (1)$$

then tangent bifurcation, also called type I intermittency [Pomeau & Manneville, 1980], occurs when a tangency develops in iterates of $F(x_n)$ across the $x_n = x_{n+1}$ reflection line. (Pitchfork bifurcations occur when iterates of $F(x_n)$ possess perpendicular crossings of this line.) Just before the tangency occurs (characterized by the closeness parameter, ϵ , being small), the map is almost tangent to the reflection line and a long channel is formed. When the iterations enter, a long laminar-like flow is established, with nearly periodic behavior. Once the iterations leave the channel, they behave chaotically, then re-enter the channel. The result is a long region of laminar flow that is intermittently interrupted by chaotic intervals. This occurs when ϵ is near zero and tangency is about to occur, hence the two names: intermittent chaos and tangent bifurcation. Experimentally, type I intermittency has been observed in turbulent fluids [Bergé *et al.*, 1980], nonlinear oscillators [Jeffries & Perez, 1982], chemical reactions [Pomeau *et al.*, 1981], and Josephson junctions [Weh & Kao, 1983]. An excellent introduction to the intermittency route to chaos is given in Schuster [1995].

In the pioneering studies [Manneville & Pomeau, 1979] and [Pomeau & Manneville, 1980], it was found that the number of iterations followed an $\epsilon^{-1/2}$ dependence and that the Lyapunov exponent varied as $\epsilon^{1/2}$ for a logistic mapping ($z = 2$). In the work by [Hirsch *et al.*, 1982], an expression for the number of iterations spent inside the channel was developed. The equation for the third iterate, i.e. $F(F(F(x)))$ or $F^{(3)}(x)$ where $F(x) = Rx(1-x)$, was expanded in a Taylor series about one of the tangency points for $R_c = 1 + \sqrt{8}$. In the case of the logistic map, we get

$$F^{(3)}(x) = x_c + (x - x_c) + a_c(x - x_c)^2 + b_c(R_c - R), \quad (2)$$

where x_c is one of the three contact points. After a transformation that centers and rescales the system around x_c ($y_n \equiv \frac{x_n - x_c}{b_c}$), the recursion relation can be put into the form

$$y_{n+1} = ay_n^2 + y_n + \epsilon, \quad (3)$$

where $\epsilon \equiv R_c - R > 0$ and $a \equiv a_c b_c$. The more general case can be studied as a first, second, or any iterate instead of just the third iterate, as long as a tangency develops. To derive an analytic description of the trajectory, [Hirsch *et. al.*, 1982] switched from a difference equation to a differential equation. Thus, they considered

$$\frac{dy}{dn} = ay^2 + \epsilon. \quad (4)$$

This approximation is justified as long as the number of iterations in the channel is large enough or, alternately, that the step size between iterations is small compared to the channel length. This is an easy differential equation to solve. One obtains

$$n(y_{in}) = \frac{1}{\sqrt{a\epsilon}} \left[\tan^{-1} \left(y_{out} \sqrt{\frac{a}{\epsilon}} \right) - \tan^{-1} \left(y_{in} \sqrt{\frac{a}{\epsilon}} \right) \right]. \quad (5)$$

“ y_{in} ” is the entrance to the tangency channel and “ y_{out} ” is the exit value and one has that

$$-y_{out} \leq y_{in} \leq y_{out}. \quad (6)$$

[Hirsch *et. al.*, 1982] observed that the entrance points for the logistic map, y_{in} ($R_c \geq R$), had a probability distribution that was roughly uniform. Given this distribution, the average number of iterations to travel the length of the channel is given as

$$\langle n \rangle \equiv \frac{1}{2y_{out}} \int_{-y_{out}}^{y_{out}} n(y_{in}) dy_{in} = \frac{1}{\sqrt{a\epsilon}} \tan^{-1} \left(y_{out} \sqrt{\frac{a}{\epsilon}} \right). \quad (7)$$

[Hirsch *et. al.*, 1982] also derived a form for the average number of iterations for an arbitrary universality class. The universality class, z , is given by the lowest non vanishing power of $(x - x_c)$ in the expansion around the tangency point. For tangency to develop, z must always be an even number:

$$y_{n+1} = ay_n^z + y_n + \epsilon. \quad (8)$$

This leads to the differential equation,

$$\frac{dy}{dn} = ay^z + \epsilon. \quad (9)$$

and to the number of iterations,

$$n(y_{in}) = a^{-1/z} \epsilon^{-1+1/z} \int_{y_{in} \sqrt[z]{\frac{a}{\epsilon}}}^{y_{out} \sqrt[z]{\frac{a}{\epsilon}}} \frac{d\bar{y}}{\bar{y}^z + 1}. \quad (10)$$

The average number of iterations is given by

$$\langle n \rangle = \frac{1}{2} a^{-1/z} \epsilon^{-1+1/z} \int_{-y_{out} \sqrt[z]{\frac{a}{\epsilon}}}^{y_{out} \sqrt[z]{\frac{a}{\epsilon}}} \frac{d\bar{y}}{\bar{y}^z + 1}, \quad (11)$$

when the entrance distribution is again uniform. The numerical simulations in [Hirsch *et al.*, 1982] agreed with predicted values quite well.

There are two manners in which Lyapunov exponents may be defined in a simulation with many trajectories. One may define a procedure which measures the Lyapunov exponent on a given trajectory, for example a single channel pass, and then averages over these trajectories. Another possibility is to measure the exponent across many trajectories or channel passes, using a binning procedure to define variances. We will use both procedures here to illustrate the theory. The first procedure will be termed a *single pass* measurement, the second a *many pass* measurement. We will develop the theory for the first procedure in the next Section, which will then be illustrated in Section 3 by a simulation in an isolated tangency channel for general z . As an illustration of a many pass measurement, a simulation of the intermittent transition in the logistic map will be described in Section 4. The modified theory will be motivated and a simple phenomenological model of the data will then be given in Section 5. In Section 6 an improved expression for the inverse number density, $\frac{dy}{dn}$ due to the discrete nature of the iterative flow will be developed. This will improve the comparison of the model to measurement. Finally, we will summarize our findings and make suggestions for further improvements in the model in the final Section.

2. Tangency Channel Theory

Our analysis of the system described by Eqs.(8) and (9) is built on the work of both [Pomeau and Manneville, 1980] and [Hirsch *et. al.*, 1982]. In contrast to the situation for the average number, $\langle n \rangle$, little work has been done to develop expressions for the Lyapunov exponents for the tangency channel in intermittent systems. We are interested in understanding the ϵ dependence of the Lyapunov exponent for $z = 2$, finding the constant of proportionality, and generalizing the results for an arbitrary universality class, z .

The Lyapunov exponent is a measurement which characterizes the sensitive dependence on initial conditions of chaotic systems. It is defined as the coefficient of the average exponential growth per unit time between initial and final states of a system, which in this case we will take to be a single pass through a tangency channel. It is given in the case of the one-dimensional mappings considered here by [Scheck, 1994]

$$\lambda \equiv \lim_{n \rightarrow \infty} \frac{1}{n} \sum_{i=1}^n \ln \left| \frac{dF(y_i)}{dy_i} \right|. \quad (12)$$

This gives us our starting point for deriving a theory for the Lyapunov exponent for a system with an arbitrary universality class. In that case, the function $F(y_i)$ from (8) is

$$F(y_i) = ay_i^z + y_i + \epsilon, \quad (13)$$

so

$$\frac{dF(y_i)}{dy_i} = 1 + azy_i^{z-1}. \quad (14)$$

Since we are interested in the Lyapunov exponent for the tangency channel, there are only a finite number of steps during which the iterations are confined to the channel and the appropriate value for n for this trajectory is the total number of iterations in the channel, $n(y_{in})$. With this in mind, the Lyapunov exponent is modeled by

$$\lambda(y_{in}) \equiv \frac{1}{n(y_{in})} \int_{y_{in}}^{y_{out}} dn \ln |1 + azy^{z-1}|, \quad (15)$$

where we have replaced the discrete sum by an integral over n -space. Again, this step is justified as long as the number of iterations is large enough so that the values of the natural logs of the slope are almost continuous.

From Eq.(9), we have

$$dn = \frac{dy}{ay^z + \epsilon}, \quad (16)$$

so that

$$\lambda(y_{in}) = \frac{1}{n(y_{in})} \int_{y_{in}}^{y_{out}} dy \frac{\ln |1 + azy^{z-1}|}{ay^z + \epsilon}. \quad (17)$$

This gives the Lyapunov exponent for the system starting at y_{in} and ending at y_{out} .

In the logistic map or any other system, the entrance into the tube is random. Since the starting points are randomly distributed, it is more useful to derive a formula for the average Lyapunov exponent per pass. Using the above formula for $\lambda(y_{in})$, we can calculate the average value of the Lyapunov exponent and obtain

$$\langle \lambda \rangle \equiv \int_{-y_{out}}^{y_{out}} dy_{in} \lambda(y_{in}) P(y_{in}), \quad (18)$$

where the probability function $P(y_{in})$ satisfies

$$\int_{-y_{out}}^{y_{out}} dy_{in} P(y_{in}) = 1. \quad (19)$$

For the present, let us consider the special case of a uniform distribution,

$$P(y_{in}) = \frac{1}{2y_{out}}. \quad (20)$$

Using this probability distribution, we obtain

$$\langle \lambda \rangle = \frac{1}{2y_{out}} \int_{-y_{out}}^{y_{out}} dy_{in} \frac{I(y_{in})}{n(y_{in})}, \quad (21)$$

where

$$I(y_{in}) \equiv \int_{y_{in}}^{y_{out}} dy \frac{\ln |1 + azy^{z-1}|}{ay^z + \epsilon}, \quad (22)$$

and where $n(y_{in})$ is given by Eq.(10) above.

One approximation and a change of variables are necessary to make this formula more usable. One important step is to define the value for y_{out} as

$$y_{out} \equiv s \sqrt[z]{\frac{\epsilon}{a}}, \quad (23)$$

where “s” is a positive scale factor that can be independently set in order to model a given system. Clearly, s can not be arbitrarily large. A natural requirement is that the derivative in (14) be positive, making the possible “throat” of the channel end at the point where $\frac{dF}{dy} = 0$. This gives that

$$s_{max} \equiv z^{\frac{1}{1-z}} a^{\frac{1}{z(1-z)}} \epsilon^{-\frac{1}{z}}, \quad (24)$$

is the maximum value of s for given z , ϵ and a . With the value of y_{out} from (23), the integral $I(y_{in})$ can be simplified with a change of variables. Let

$$y' = \frac{y}{y_{out}}. \quad (25)$$

Therefore

$$I(y_{in}) = s a^{-\frac{1}{z}} \epsilon^{-1+\frac{1}{z}} \int_{\frac{y_{in}}{s \sqrt[z]{\frac{\epsilon}{a}}}}^1 dy' \frac{\ln(1 + z a^{\frac{1}{z}} \epsilon^{1-\frac{1}{z}} s^{z-1} y'^{z-1})}{s^z y'^z + 1}, \quad (26)$$

where the absolute value in the natural log is no longer necessary. The Taylor series expansion for natural log is ($|x| < 1$)

$$\ln(1 + x) = x - \frac{x^2}{2} + \frac{x^3}{3} - \frac{x^4}{4} + \dots \quad (27)$$

Using this approximation we have simply

$$I(y_{in}) \approx z s^z \int_{\frac{y_{in}}{s \sqrt[z]{\frac{\epsilon}{a}}}}^1 dy' \frac{y'^{z-1}}{s^z y'^z + 1} = \ln \left(\frac{s^z + 1}{\frac{a}{\epsilon} y_{in}^z + 1} \right), \quad (28)$$

as long as

$$s \ll s_{max}. \quad (29)$$

Our simplified formula for the average Lyapunov exponent is now

$$\langle \lambda \rangle = \frac{1}{2s} a^{2/z} \epsilon^{1-2/z} \int_{-y_{out}}^{y_{out}} \frac{dy_{in}}{\int_{s\hat{y}}^s \frac{d\hat{y}}{\hat{y}^z+1}} \ln \left(\frac{s^z + 1}{\epsilon y_{in}^z + 1} \right). \quad (30)$$

We now make the same scale change in the y_{in} integral as in the y integral in (25):

$$\hat{y} \equiv \frac{y_{in}}{y_{out}}. \quad (31)$$

Therefore

$$\langle \lambda \rangle = \frac{1}{2} a^{1/z} \epsilon^{1-1/z} \int_{-1}^1 \frac{d\hat{y}}{\int_{s\hat{y}}^s \frac{d\hat{y}}{\hat{y}^z+1}} \ln \left(\frac{s^z + 1}{s^z \hat{y}^z + 1} \right). \quad (32)$$

As one can see, for constant s the average Lyapunov exponent varies as $\epsilon^{1-1/z}$ with a constant of proportionality determined by the parameters a and s . In the case where $z = 2$ this gives

$$\langle \lambda \rangle = \frac{1}{2} \sqrt{a\epsilon} \int_{-1}^1 \frac{d\hat{y}}{\tan^{-1}(s) - \tan^{-1}(s\hat{y})} \ln \left(\frac{s^z + 1}{s^z \hat{y}^z + 1} \right). \quad (33)$$

For a general probability distribution, we would have instead

$$\langle \lambda \rangle = a^{1/z} \epsilon^{1-1/z} \int_{-1}^1 d\hat{y} \frac{P(\hat{y})}{\int_{s\hat{y}}^s \frac{d\hat{y}}{\hat{y}^z+1}} \ln \left(\frac{s^z + 1}{s^z \hat{y}^z + 1} \right) d\hat{y}, \quad (34)$$

where

$$\int_{-1}^1 d\hat{y} P(\hat{y}) = 1. \quad (35)$$

In the case of constant scale factor s , we therefore see that the single pass tangency channel Lyapunov exponent behaves like $\epsilon^{1-1/z}$.

3. Tangency Channel Simulation

The integral in Eq.(33) was calculated using numerical methods and compared against numerical simulations of the logistic map ($z = 2$). In all cases we used a simulation consisting

of 10,000 Monte Carlo runs for each data point. As can be seen in Figs.1-3, for values of $s = 0.1, 1.0$ and 10 , the theoretical values agree with the simulation values for a uniform probability distribution for small enough ϵ . At low ϵ , the agreement is excellent, with the theoretical value straddled by the upper and lower error values of the simulation. In the $s = 0.1$ simulation, the assumption that the discrete sum can be approximated by a continuous integral breaks down at large enough ϵ due to the very small number of iterations in the channel. For the $s = 10$ simulation, the natural log approximation, Eq.(27), starts to break down and is the main cause of the divergence between theory and simulation. The least divergence between theory and simulation occurs when $s \approx 1$. The calculations become more time consuming at larger s due to the increased number of iterations necessary to pass through the channel.

We examined the more general expression, Eq.(34), when $z = 2$ for other probability distributions including a Gaussian and a $|y|$ distribution of normal deviates. Although these results are not illustrated here, the theoretical and simulation results were again in excellent agreement for small enough ϵ . We also examined the ϵ dependence for higher universality classes. However, due to the large amount of computer time it takes to do such simulations, we have data only for one additional z value. For a universality class of $z = 4$, the Lyapunov dependence should be $\epsilon^{3/4}$, which is clearly confirmed in Fig. 4.

The Section 2 expressions for $\langle \lambda \rangle$ are displayed in a form appropriate for a simulation at a fixed value of the scale, s . However, the approximation employed, Eq.(29), is simply the condition that the channel length be much smaller than the total gate size (determined by the tangency point and the point at $\frac{dF}{dy} = 0$). Thus, the expression Eq.(34) holds also for a fixed tangency channel fraction, f ,

$$f \equiv \frac{y_{out}}{(az)^{\frac{1}{1-z}}} = s\epsilon^{\frac{1}{z}} z^{\frac{1}{z-1}} a^{\frac{1}{z(z-1)}}, \quad (36)$$

as long as

$$f \ll 1. \quad (37)$$

The quantity $(az)^{\frac{1}{1-z}}$ is just the total model gate size. For $z = 2$ the relationship between f and s is simply

$$f = 2s\sqrt{a\epsilon}. \quad (38)$$

When the change from s to f is made in Eq.(34), the result is no longer proportional to $\epsilon^{1/2}$ but in fact goes to a constant at small values of ϵ . Mathematically, this is due to the fact that the denominator, proportional to the number of iterates in the channel for a starting position \hat{y} , falls off like $\epsilon^{1/2}$ when $\hat{y} \approx 1$. Physically, the Lyapunov exponent is being dominated by the small number of iterates associated with entrances on the far side of the narrow channel. Fig. 5 shows the predicted and measured values of the Lyapunov exponent, $\langle \lambda \rangle$ for the case $f = 0.1$, i.e., the channel length is one-tenth the size of the gate, when the entrance probability is again uniform. As expected, and unlike the cases presented above at fixed s , the value of the Lyapunov exponent becomes constant at small ϵ , the theoretical value remaining about 10% larger than simulation. This amount of deviation is what we would expect since the term kept in the expansion of the natural log in Eq.(27) is of order f and the first neglected term is of order f^2 . Measurements at fixed f will be important for the simulations done in the full logistic map to be considered in the next Section.

4. Logistic Map Simulation

As was pointed out earlier, there are two manners in which Lyapunov exponents can be defined in channel simulations, which we called the single pass and many pass definitions. We have already described and illustrated a single pass simulation. As an example of a many pass situation, we consider a simulation of the tangency gates in the logistic map. In doing so, we find it convenient to first describe the details and results of the numerical simulation. The theory and the model used to fit to the data will then be developed together in Section 5.

As outlined in the Introduction, the equation for the third iterate of the logistic map for

small ϵ may be expanded in a Taylor series about each of the tangency points. The positions of the tangency points are given to high precision in Table I. (Knowledge of any one gives the others through the basic recurrence relation.) Expanding to third order in $(x - x_c)$, one has for the third iterate,

$$F^{(3)}(x) = x_c + (x - x_c) + a_c(x - x_c)^2 + c_c(x - x_c)^3 + b_c(R_c - R). \quad (39)$$

The values of a_c , b_c and c_c are given in Table I. Again introducing $y_n = \frac{x_n - x_c}{b_c}$, the difference equation for all three of the gates takes the form (note that $c_c b_c^2 = -196$ to high accuracy for all gates),

$$y_{n+1} - y_n = \epsilon + a y_n^2 - \frac{2}{49} a^2 y_n^3, \quad (40)$$

where the constant “a” takes on the value

$$a = 69.29646455628 \dots \quad (41)$$

An interesting aspect of the simulation is the exclusion of certain x -values from the logistic map at finite ϵ . We have labeled the tangency gates in increasing order of their x_c values. Referring to the third iterate map, shown for $\epsilon = 0$ in Fig. 6, it is clear by drawing a horizontal line that gate 1 is reachable only under steady-state conditions from points close to point C in the Figure. Likewise, gate 3 is reachable only from previous iterates starting on or near points A or B in the figure. (Since $x = 0.5$ is a symmetry point in the mapping, the values of $F^{(3)}(x)$ at points A and B are the same.) Note in this context that the laminate flow through gates 1 and 2 is from smaller x -values to larger ones, whereas the flow through gate 3 is in the opposite direction. Iterates entering gate 1 from the point C will actually enter at the value $x_L \equiv F^{(3)}(x_C)$; points between $x = 0$ and $x = x_L$ will never be reached. This is after a possible transient of a single iteration. Likewise, iterates entering gate 3 from points A and B will enter at the value $x_R \equiv F^{(3)}(x_{A,B})$; points between $x = x_R$ and $x = 1$ are never reached, again after a possible 1-iteration transient. By drawing a horizontal line, gate 2 is seen to be reachable from 4 separate x -regions (excluding the points to the left of x_L and to the right of x_R).

The measurements leading to values and variances of the Lyapunov exponents were taken from a single trajectory of 1.6 million iterations of the third-iterate logistic map at each $\epsilon^{1/2}$ value following an initial “heating” to remove the transient x -values. Monte Carlo error bars for the Lyapunov exponents were then measured by breaking the single trajectory into 100 bins. Runs were made both at fixed gate fraction, f , as well as at fixed scale factor, s .

Fig. 7 shows a \log_{10} plot of the contribution of each of the three gates when the fraction of the gate being measured is $f = 0.1$, the same used in Fig. 5. Note that $f = 0.1$ indicates the fraction of the model gate size, characterized by Eq. (3), not the actual gate size. The ratio of the model to actual gate length is about 1.025. The gate Lyapunov exponents, $\langle \lambda \rangle_g$, are normalized to the number of third-iterate hits within each gate, which at small ϵ just approaches 1/3 of the total iterations. We notice that even at the larger ϵ values the contribution from different gates is the same within errors.

Fig. 8 shows the contribution of each of the three gates to the Lyapunov exponent, $\langle \lambda \rangle_g$, in a simulation with a fixed value of the scale factor, $s = 1.0$. Eq.(7) implies that such a simulation will have a mixture of half iterations inside the gates and half outside, as indeed is observed. The error bars here are larger in a relative sense than in Fig. 7 because the gate size is shrinking like $\epsilon^{1/2}$ (see Eq.(23)), leading to smaller statistics. Also unlike Fig. 7 there are significantly different contributions from the three gates at larger ϵ values, the middle gate having an enhanced $\langle \lambda \rangle_g$. It is only at values of ϵ below and including $\epsilon^{1/2} = 0.512 \times 10^{-3}$ that a distinction between the gates can no longer be seen. However, this may simply be the result of the larger statistical fluctuations present at smaller ϵ .

Note that the fixed f data in Fig. 7 shows an approximate $\epsilon^{1/2}$ behavior, while the fixed s simulation in Fig. 8 behaves approximately as ϵ at small ϵ values. These behaviors are in contrast to the simulations in Section 3 where the fixed f data went to a constant at small ϵ and the fixed s data behaved like $\epsilon^{1/2}$. The ϵ behavior of the logistic map Lyapunov exponents will be commented on further in the next Section.

In order to model the Lyapunov exponents for the gates, it is necessary to have an understanding of the entrance probability for the gates as a function of position in the gate.

There are two ways in which a laminate flow may begin in the tangency channel. Primarily, entrance into the gate occurs as a continuous flow from just outside the gate. Alternatively, the flow can begin in a discontinuous fashion from a disjoint region of the map. These two entrance routes will be termed the *continuous* and *discontinuous* types, respectively. Fig. 9 presents a measurement of the binned discontinuous entrance rate, n_d , for the first gate of the $f = 0.1$ simulation at $\epsilon^{1/2} = 0.128 \times 10^{-3}$. The data is divided into 19 bins with bin size of $\Delta x_{bin} = 0.5624 \times 10^{-4}$, which is just the model gate width divided by 100. The first bin (which would have extended from -10 to -9 in the figure units) contains both continuous and discontinuous entrances. Since we have not attempted to separate the discontinuous from the continuous entrances in this bin and because the total rate is off scale, this first bin is not shown. The entrance rate seems to be fairly uniform in this Figure; gate 2 and (the mirror image of) gate 3 look very similar. This approximate entrance uniformity for small f will be useful in setting up a simple model of the gate contribution to the Lyapunov exponent, which will be described in the next Section.

5. Simple Model

We will now develop theoretical expressions for the ϵ -dependence of the Lyapunov exponents for the logistic map. For this purpose we need to develop expressions for $\langle n \rangle$ and $\langle \lambda \rangle$ in a many pass simulation, as opposed to the single pass considerations in Sections 2 and 3. In a many pass simulation, the number of iterations in the gate will be weighted by the entrance *rate* rather than probability. Therefore, Eq.(7), generalized to an arbitrary probability distribution, is replaced with

$$\langle n \rangle_g = \frac{1}{2} \int_{-1}^1 d\hat{y} \frac{dN(\hat{y})}{d\hat{y}} n(y_{in}), \quad (42)$$

where

$$n(y_{in}) = \frac{1}{\sqrt{a\epsilon}} \left(\tan^{-1}\left(\frac{f}{2\sqrt{a\epsilon}}\right) - \tan^{-1}\left(\frac{f\hat{y}}{2\sqrt{a\epsilon}}\right) \right). \quad (43)$$

We also are using the dimensionless variable \hat{y} introduced in Eq.(31) ($y_{in} = \hat{y}y_{out}$). The functional form of $\frac{dN(\hat{y})}{d\hat{y}}$ has yet to be specified. Note that n_d in Fig. 9 is given by $n_d = \frac{dN(\hat{y})}{d\hat{y}}\Delta\hat{y}_{bin}$ where in this case $\Delta\hat{y}_{bin} = 0.1$.

The form for the Lyapunov exponent, Eqs.(21) and (22), must also be modified. It is again the rate rather than the probability which is relevant. In addition, for a many pass simulation the Lyapunov integrand in Eq.(21) must be weighted by the ratio of the number of iterations for each passage through the channel, $n(y_{in})$, to the average total number of iterations, $\langle n \rangle_g$, resulting in

$$\langle \lambda \rangle_g = \frac{1}{2 \langle n \rangle_g} \int_{-1}^1 d\hat{y} \frac{dN(\hat{y})}{d\hat{y}} I(y_{in}), \quad (44)$$

where

$$I(y_{in}) = \frac{2}{f} \int_{\hat{y}}^1 dy' \frac{\ln(1 + fy')}{y'^2 + \frac{4a\epsilon}{f^2}}. \quad (45)$$

Making the same approximation as in Eq.(27) above, this simplifies to

$$\langle \lambda \rangle_g = \frac{1}{2 \langle n \rangle_g} \int_{-1}^1 d\hat{y} \frac{dN(\hat{y})}{d\hat{y}} \ln \left(\frac{1 + \frac{4a\epsilon}{f^2}}{\hat{y}^2 + \frac{4a\epsilon}{f^2}} \right). \quad (46)$$

We use f instead of s in these formulas since most of the simulations in the following will use fixed f .

As we have seen in the last Section, the Lyapunov exponents from the three gates are apparently indistinguishable at small enough ϵ . A very useful simplification therefore is to ignore the distinction between the gates and model the Lyapunov exponent as if there were only two regions, the gate (or periodic) region and the outside (or chaotic) region. In addition, Fig. 9 suggests that a reasonable model of the channel region is to assume that the discontinuous entrance rate is uniform. This last simplification is only possible for small enough f , the entrance rate in the complete tangency channels being far from uniform. These assumptions will allow us to construct a very simple model of the ϵ dependence of the Lyapunov exponents. The choice of $f = 0.1$ to separate the two regions is arbitrary. A smaller value would result in an even more uniform entrance rate than Fig. 9; however,

one would also lose statistics because of the smaller gate size. As we will see, the gate fraction f will be used to formally separate the outside and inside gate Lyapunov exponent behaviors.

A new aspect of modeling the actual gates of the logistic map is the fact that the entrance to the gates can be from flow further up the channel or from a completely disjoint part of the map. These possibilities were termed the continuous and discontinuous routes in the last Section. One may show that the continuous entrances occur within a scaled distance of $\sim f/2 + 2a\epsilon/f$ from the lower limit (-1) of the integrals in Eqs.(42) and (44). In Fig. 9 this contribution would extend about halfway through the first (deleted) bin. Since these entrances always occur in a narrow range of the integrations in these equations for the range of ϵ considered, it is reasonable to model this contribution by a Dirac delta function located at the lower limit, $\hat{y} = -1$. In addition, we saw in Fig. 9 that the discontinuous part of the entrance rate was approximately uniform. Thus we will model the entrance rate with

$$\frac{dN(\hat{y})}{d\hat{y}} = 2N_c\delta(\hat{y} + 1) + \frac{dN_d}{d\hat{y}}, \quad (47)$$

where N_c and $\frac{dN_d}{d\hat{y}}$ are constants in \hat{y} . This gives a simple model of the contributions to $\langle n \rangle_g$ and $\langle \lambda \rangle_g$ from the logistic gates:

$$\langle n \rangle_g = \frac{1}{\sqrt{a\epsilon}} \tan^{-1}\left(\frac{f}{2\sqrt{a\epsilon}}\right) \left(2N_c + \frac{dN_d}{d\hat{y}}\right), \quad (48)$$

$$\langle \lambda \rangle_g = \frac{1}{2\langle n \rangle_g} \frac{dN_d}{d\hat{y}} \int_{-1}^1 d\hat{y} \ln \left(\frac{1 + \frac{4a\epsilon}{f^2}}{\hat{y}^2 + \frac{4a\epsilon}{f^2}} \right). \quad (49)$$

Notice that N_c drops out of the expression for $\langle \lambda \rangle_g$. In fitting the data, we also need the expression for the small ϵ limit of Eq.(48), which we will call n_T :

$$n_T \equiv \frac{\pi}{2\sqrt{a\epsilon}} \left(2N_c + \frac{dN_d}{d\hat{y}}\right). \quad (50)$$

As pointed out previously, f represents a separation parameter for the gate and outside regions. Inside the gates one expects from the previous results that the number of iterations associated with a given traverse of the gate will increase like $\epsilon^{-1/2}$ at small ϵ , independent of

the form of the entrance probability. Thus in the many pass simulations of the full logistic map, one expects any given fraction f of the gates at small ϵ to eventually contain essentially all iterates. This means from Eq.(50) that the quantity $2N_c + \frac{dN_d}{d\hat{y}}$ must scale like $\epsilon^{1/2}$ for n_T to become constant. This behavior will be assumed for these quantities individually. In addition, we assume that for small enough gate fraction the continuous entrance rate is uniform. Given these assumptions, the parameters N_c and $\frac{dN_d}{d\hat{y}}$ can be parameterized as,

$$N_c \equiv \sqrt{a\epsilon}(1-f)n_T K_c, \quad (51)$$

$$\frac{dN_d}{d\hat{y}} \equiv \sqrt{a\epsilon}f n_T K_d, \quad (52)$$

where K_c and K_d are constants.

We can now better understand the ϵ dependencies in the Lyapunov exponents in the logistic map simulation seen in the last Section. For a many pass simulation we expect the model Lyapunov exponent from Eqs.(49) and (52) for fixed f to behave like $\epsilon^{1/2}$ at small ϵ . This is because $\langle n \rangle_g$ saturates to the value n_T while the rate in Eq.(52) goes like $\epsilon^{1/2}$. In contrast, for fixed scale s the exponent now acquires an extra $\epsilon^{1/2}$ factor from the gate fraction f in (52) and is expected to decrease like ϵ , as was seen in the actual simulations. This is just a result of the shrinking gate size of the fixed s simulation.

As a result of the number flow into the gate regions as ϵ decreases, the outside region becomes sparsely visited, but with the same local density of iterates. (The shape of the outside region changes very little for small ϵ .) This implies the Lyapunov exponent measured in the outside region will go to a constant for small ϵ . The flows being described are all due to the result Eq.(10) for $n(y_{in})$ and can be thought of as applications of the renormalization flow arguments, without external noise, in [J. E. Hirsch *et. al.*, 1982] and [B. Hu and J. Rudnick, 1982].

Although the emphasis here is on the gate Lyapunov exponents, one can now make a rough model of the complete logistic map exponent. Letting $\langle \lambda \rangle_g$ represent the Lyapunov exponent expression for the fixed f gate (laminar region) from Eq.(49) and $\langle \lambda \rangle_o$ be the outside (chaotic region) contribution, the expression for the Lyapunov exponent for the

complete logistic map in this model is

$$\langle \lambda \rangle^{3rd} = \frac{n_o}{n_T} \langle \lambda \rangle_o + \frac{n_g}{n_T} \langle \lambda \rangle_g, \quad (53)$$

where $n_o + n_g = n_T$. That is, $\langle \lambda \rangle^{3rd}$ is just assumed to be a sum of the exponents $\langle \lambda \rangle_g$ and $\langle \lambda \rangle_o$ weighted by the relative number of iterations spent in the two regions. A more fundamental description of the logistic map would independently calculate $\langle \lambda \rangle_o$. However, from the previous arguments we expect $\langle \lambda \rangle_o$ to simply be a constant at small ϵ . It will be evaluated from a fit to the data.

Numerically, the gate contribution in Eq.(53) is only about 1% of the total through most of the ϵ range considered for $f = 0.1$. Both terms in Eq.(53) go like $\epsilon^{1/2}$, but in different ways. The outside term behaves like $\epsilon^{1/2}$ because the outside number n_o has this dependence; the gate term also behaves this way because $\langle \lambda \rangle_g$ itself goes like $\epsilon^{1/2}$ at fixed f as explained above. Note that all Lyapunov exponents in Eq.(53) are normalized to the number of third-iterate steps in the simulation. This is symbolized by writing $\langle \lambda \rangle^{3rd}$ for the complete logistic map Lyapunov exponent. We must remember to divide this value by three to calculate the usual single-iterate value:

$$\langle \lambda \rangle^{1st} = \frac{1}{3} \langle \lambda \rangle^{3rd}. \quad (54)$$

Fig. 10 presents the results of fitting Eq.(49) to the data for the $f = 0.1$ gate exponent and Fig. 11 gives the measured and model $\langle \lambda \rangle^{1st}$ values for the complete logistic map. There are three parameters needed to do these fits: K_c , K_d and $\langle \lambda \rangle_o$. To evaluate these constants we simply fit the values of these expressions to the measured values of $\langle \lambda \rangle^{1st}$ and $\langle \lambda \rangle_g$ at a value of $\epsilon^{1/2} = 0.128 \times 10^{-3}$, near the middle of the exponential range in these figures, as well as the maximum number of gate iterations, n_T . Since we are averaging over the properties of all three gates, $n_T = \frac{1}{3} \times 1.6 \times 10^6$ for the simulation in Section 4. This gives $K_c = 0.358 \times 10^{-2}$, $K_d = 0.739 \times 10^{-2}$ and $\langle \lambda \rangle_o = 0.962$.

Of course since Figs. 10 and 11 were used to fit the model parameters, we need an independent test of how well the model truly represents the data. For this purpose we also

present Fig. 12 and Table II. Fig. 12 compares the model results against the data for a $s = 1.0$ simulation. As explained above, this data falls like ϵ . The theoretical results are satisfactory although seem somewhat high compared to measurement. In addition in Table II we give the fit results for the rates N_c and $\frac{dN_d}{d\hat{y}}$ compared to measurement. The measured value for $\frac{dN_d}{d\hat{y}}$ is actually just an average over all three gates of binned data similar to Fig. 9, and the value for N_c is the average value in the three entrance bins minus the average of the entrances in the other bins. The results for N_c are good but the fit values of $\frac{dN_d}{d\hat{y}}$ are approximately a factor of 2 larger than measurement. As we will see in the next Section, this is largely the result of an inaccurate characterization of the inverse number density, $\frac{dy}{dn}$.

6. Improved Model

Although the expression for the inverse number density, Eq.(9), is symmetric (even) in y for $z = 2$, there are at least three sources of asymmetry in the actual gate. First, the discontinuous entrance rate $\frac{dN_d}{d\hat{y}}$ raises the value of the hit density on the exit sides of all three gates. Second, the term proportional to $(x - x_c)^3$ in Eq.(39) shows that there is a small intrinsic asymmetry in the shape of the gates themselves, raising the hit density in the same sense. Most interestingly, there is also a contribution due to the finite step size of the laminar flow through the gates which contributes even for a perfectly symmetric gate. This will now be described.

Remembering that a finite difference gave rise to the left hand side of Eq.(9), a more accurate differential characterization of the iterative flow is

$$\frac{dy}{dn} + \frac{1}{2} \frac{d^2y}{dn^2} = ay^2 + \epsilon. \quad (55)$$

We will use the method of successive approximants to evaluate the second derivative term.

To zeroth order,

$$\left. \frac{dy}{dn} \right|_0 = ay^2 + \epsilon. \quad (56)$$

Thus the lowest order result for the second derivative is just

$$\frac{d^2y}{dn^2}|_0 = 2ay(ay^2 + \epsilon). \quad (57)$$

Inserting this back into the starting point, Eq.(55), we now have the improved result

$$\frac{dy}{dn}|_1 = ay^2 + \epsilon(1 - ay) - a^2y^3. \quad (58)$$

With this improvement, a better formula for the gate Lyapunov exponent is given by

$$\begin{aligned} \langle \lambda \rangle_g &= \frac{2N_c}{\langle n \rangle_g} \int_{-1}^1 dy' \frac{y'}{y'^2 + \frac{4a\epsilon}{f^2}(1 - \frac{f}{2}y') - \frac{f}{2}y'^3} \\ &+ \frac{dN_d}{d\hat{y}} \frac{1}{\langle n \rangle_g} \int_{-1}^1 d\hat{y} \int_{\hat{y}}^1 dy' \frac{y'}{y'^2 + \frac{4a\epsilon}{f^2}(1 - \frac{f}{2}y') - \frac{f}{2}y'^3}. \end{aligned} \quad (59)$$

Note that the intrinsic contribution to the inverse hit rate from Eq.(40) is of the same sign but 49/2 times smaller than the term from Eq.(58) and so is neglected. (The intrinsic term would also slightly alter the numerator; see Eq.(12).)

Notice that the continuous entrance term, N_c , now *does* contribute to the expression for $\langle \lambda \rangle_g$ since the inverse number density is no longer an even function. Unfortunately, the inner integral can no longer be done analytically and a double integral survives. Because the emphasis here is on modeling the Lyapunov exponent and because of the difficulty of performing the numerical integration leading to n_T at small values of ϵ , we have not attempted to make the same correction in the expression for $\langle n \rangle_g$. Thus, we continue to use the expression Eq.(48) above for $\langle n \rangle_g$ in the gate region.

When the same sort of fit is made to the simulation data as in Section 5, there is surprisingly little change in the functional forms in Figs. 10, 11 and 12, although the inverse number rates of the two models are considerably different and the N_c term is now contributing about 50% of the total. The new fit gives $K_c \simeq K_d = 0.379 \times 10^{-2}$. (The value of $\langle \lambda \rangle_o$ does not change from the previous fit.) The major improvement occurs in the value of the discontinuous entrance density, $\frac{dN_d}{d\hat{y}}$ (see the ‘‘Improved model’’ columns of Table II), which is now within 5% of the measured value at $\epsilon^{1/2} = 0.128 \times 10^{-3}$, where the fit is actually made. However, the value for N_c has increased and is now approximately 6% large compared to the measured value. (Note that $2N_c + \frac{dN_d}{d\hat{y}}$ in Table II is required to have the same value in the

two models because the form for $\langle n \rangle_g$ is unchanged.) This problem should be cured when the more accurate result for the number density implied by Eq.(58) is used in the expression for $n(y_{in})$ in Eq.(10).

7. Summary and Conclusions

Tangent bifurcation or intermittent chaos is a common occurrence in systems that exhibit chaotic behavior. In these systems the intermittent behavior can be modeled by differential and difference equations of some universality class. We found that the Lyapunov exponent for isolated gates at single channel pass can be modeled given the universality class, the parameters of the difference equation, the scale factor s or fraction f of the gate size, and the closeness factor ϵ . Our main theoretical result for these systems, subject to the restriction of a sufficient number of steps in the channel and the small gate approximation in Eqs.(29) or (37), is that the average Lyapunov exponent is given by Eqs.(34) and (35). Single pass numerical simulations were consistent with these expressions. At fixed scale factor s these results gave a Lyapunov exponent proportional to $\epsilon^{1-1/z}$ for a tangency channel with general universality class, z . We also showed that a simulation at fixed gate fraction f gave a result which instead became constant at small values of ϵ for $z = 2$ due to a small number of entrances on the far side of the narrow channel.

Simulations were also performed on the full logistic map near the intermittent transition at $R = 1 + \sqrt{8}$. Modified expressions for the gate number, Eq.(42), and Lyapunov exponent, Eq.(46), for a many channel pass simulation were motivated. A new aspect encountered in the description of the actual tangency channels was the existence of a continuous flow contribution into the tangency gate. Two phenomenological models of the channel were constructed and examined. A very simple model was considered which was able to give a fairly realistic characterization of the various Lyapunov exponents and the continuous, N_c , and discontinuous, $\frac{dN_d}{dij}$, entrance parameters. We also derived a first-order correction to the inverse hit rate due to the discrete nature of the iterative flow, which mainly improved the

comparison with the measured discontinuous entrance parameter.

Besides applying the finite discretization correction to the number density expression, there is considerable room for improving the present model of the logistic gates. For example, the modeling of the continuous contribution to the gates as a delta function is clearly oversimplified; no attempt has made no attempt to resolve the shape of the continuous entrance rate in the binning procedure of Fig. 9. In addition, the approximation used for the logarithm, Eq.(27), can be removed at the cost of a more complicated numerical evaluation. Finally, further discretization corrections to both $\langle \lambda \rangle_g$ and $\langle n \rangle_g$ should result in an improved characterization of the inverse number density, leading to better comparison with the measured rates and functional behaviors at larger ϵ values.

Acknowledgments

This work was supported in part by NSF Grants PHY-9424124 and PHY-9722073. Some of the numerical calculations were performed on the Power Challenge Array at the National Center for Supercomputing Applications.

References

- Bergé, P., Dubois, M., Manneville, P., & Pomeau, Y. [1980], “Intermittency in Rayleigh-Bénard Convection”, *J. Physique Lett.* **41**, L341-L354.
- Hirsch, J. E., Hubermann, B. A. & Scalapino, D. J. [1982] “Theory of Intermittency”, *Phys. Rev.* **A25**, 519-532.
- Hirsch, J.E. & Nauenberg, M. [1982], “Intermittency in the Presence of Noise: A Renormalization Group Formulation”, *Phys. Lett.* **87A**, 391-393.
- Hu, B. & Rudnick, J. [1982], “Exact Solutions to the Feigenbaum Renormalization-Group Equations for Intermittency”, *Phys. Rev. Lett.* **48**, 1645-1648.
- Jeffries, C. & Pérez, J. [1982], “Observation of a Pomeau-Manneville Intermittent Route to Chaos in a Nonlinear Oscillator”, *Phys. Rev.* **A26**, 2117-2122.
- Manneville, P. & Pomeau, Y. [1979] “Intermittency and the Lorenz Model”, *Phys. Lett.* **75A**, 1-2.
- Pomeau, Y. & Manneville, P. [1980] “Intermittent Transition to Turbulence in Dissipative Dynamical Systems”, *Commun. Math. Phys.* **74**, 189-197.
- Pomeau, Y., Roux, J. C., Rossi, A., Bachelart, S. & Vidal, C. [1981], “Intermittent Behavior in the Belousov-Zhabotinsky Reaction”, *J. Physique Lett.* **41**, L271-L273.
- Scheck, F. A. [1994] *Mechanics* (Springer, Berlin) 2nd ed., p. 371.
- Schuster, H. G. [1995] *Deterministic Chaos* (VCH, Weinheim) 3rd ed., pp. 79-102.
- Weh, W. J., & Kao, Y. H. [1983], “Intermittency in Josephson Junctions”, *Appl. Phys. Lett.* **42**, 299-301.

TABLES

TABLE I. Values of the tangency points, x_c , and the constants a_c , b_c and c_c in Eq.(39).

	x_c	a_c	b_c	c_c
gate 1	0.1599288184463...	88.91012989368...	0.7793989800616...	-322.6535182739...
gate 2	0.5143552770620...	34.14530797001...	2.029457886780...	-47.58783903539...
gate 3	0.9563178419736...	-310.6483669763...	-0.2230704292148...	-3938.873792041...

TABLE II. Results from two models for the continuum number contribution, N_c , and the discontinuous number density, $\frac{dn}{dy}$ when $f = 0.1$.

$\epsilon^{1/2}$	Simulation		Simple model		Improved model	
	N_c	$\frac{dN_d}{dy}$	N_c	$\frac{dN_d}{dy}$	N_c	$\frac{dN_d}{dy}$
0.8×10^{-5}	$0.1021(6) \times 10^2$	$0.112(5) \times 10^1$	0.101×10^2	0.232×10^1	0.107×10^1	0.119×10^1
0.16×10^{-4}	$0.2028(8) \times 10^2$	$0.224(6) \times 10^1$	0.203×10^2	0.464×10^1	0.214×10^2	0.237×10^1
0.32×10^{-4}	$0.403(1) \times 10^2$	$0.466(8) \times 10^1$	0.406×10^2	0.927×10^1	0.429×10^2	0.474×10^1
0.64×10^{-4}	$0.804(2) \times 10^2$	$0.93(2) \times 10^1$	0.812×10^2	0.185×10^2	0.857×10^2	0.949×10^1
0.128×10^{-3}	$0.1607(2) \times 10^3$	$0.181(2) \times 10^2$	0.162×10^3	0.371×10^2	0.171×10^3	0.190×10^2
0.256×10^{-3}	$0.3181(3) \times 10^3$	$0.368(2) \times 10^2$	0.325×10^3	0.742×10^2	0.343×10^3	0.380×10^2
0.512×10^{-3}	$0.6274(4) \times 10^3$	$0.718(4) \times 10^2$	0.649×10^3	0.148×10^3	0.686×10^3	0.759×10^2
0.1024×10^{-2}	$0.1216(1) \times 10^4$	$0.1411(5) \times 10^3$	0.130×10^4	0.297×10^3	0.137×10^4	0.152×10^3
0.2048×10^{-2}	$0.2297(1) \times 10^4$	$0.2623(7) \times 10^3$	0.260×10^4	0.594×10^3	0.274×10^4	0.304×10^3
0.4096×10^{-2}	$0.4135(2) \times 10^4$	$0.4769(9) \times 10^3$	0.519×10^4	0.119×10^4	0.548×10^4	0.607×10^3

Figure Captions

1. Simulation of the system described by Eq.(8) compared to the Lyapunov exponent given by Eq.(33) ($z = 2$; uniform entrance probability). We plot $\log_{10} \langle \lambda \rangle$ against $\log_{10} \epsilon^{1/2}$; the prediction (33) is given by the dotted line. The Monte Carlo error bars on the calculation are extremely small and are given by the data point bars. We are using $a = 34$ (the same as in [Hirsch *et. al.*, 1982]) and $s = 0.1$, with $\epsilon^{1/2}$ ranging in value from 0.8×10^{-5} upwards by factors of 2.
2. The same as Fig. 1 but for $s=1$.
3. The same as in Fig. 1 except for $s = 10$. Note that the largest $\epsilon^{1/2}$ value, present in Figs. 1 and 2, violates the bound $s < s_{max}$ of the text and has been excluded.
4. The case of $z = 4$, $s = 0.1$ $a = 34$ and uniform entrance probability.
5. Contribution to the Lyapunov exponent, as a function of $\log_{10} \epsilon^{1/2}$, from a simulation involving 10,000 gate entrances when f , the gate fraction, is set to 0.1, the entrance probability is uniform and $a = 34$. The theoretical result from Eq.(33) is given by the dotted line.
6. The third iterate of the logistic equation, $F^{(3)}(x)$, as a function of x when $\epsilon = 0$. The three points where the third iterate makes tangential contact with the 45-degree line are the tangency points. The points A, B and C in the map are discussed in the text.
7. Contributions of the three tangency gates to the logistic map Lyapunov exponent, $\langle \lambda \rangle_g$ for $f = 0.1$. Gate 1 data is given by the circles, gate 2 by the squares and gate 3 by the triangles. Note that the ordinate values of the gate 1 and 3 data points have been shifted to the left and right, respectively, for clarity of presentation.
8. Contributions of the three tangency gates to the logistic map Lyapunov exponent, $\langle \lambda \rangle_g$ for $s = 1.0$. The meaning of the symbols is the same as in Fig. 7.

9. The number of discontinuous entrances, n_d , for gate 1 when $f = 0.1$ and $\epsilon^{1/2} = 0.128 \times 10^{-3}$ as a function of bin number centered about the first tangency point, x_c . Each data point above corresponds to entrances in a bin size of $\Delta x_{bin} = 0.5624 \times 10^{-4}$. (The bin extending from -10 to -9 is not shown; see the text.)
10. Comparison of the model results for the Lyapunov exponent for the $f = 0.1$ simulation with the averaged data from Fig. 7. The model values, given by a dotted line (simple model) and a solid line (improved model), are indistinguishable. The data point at $\log_{10}(0.128 \times 10^{-3}) = -3.893 \dots$ is used for the fit.
11. Comparison of the model results for the Lyapunov exponent (1st iterate) for the entire map with the data. The model values, given by a dotted line (simple model) and a solid line (improved model), are again indistinguishable. The data point at $\log_{10}(0.128 \times 10^{-3}) = -3.893 \dots$ is used for the fit.
12. Comparison of the model results for the Lyapunov exponent for the $s = 1.0$ simulation with the averaged gate data from Fig. 8. The model values are given by a dotted line (simple model) and a solid line (improved model).

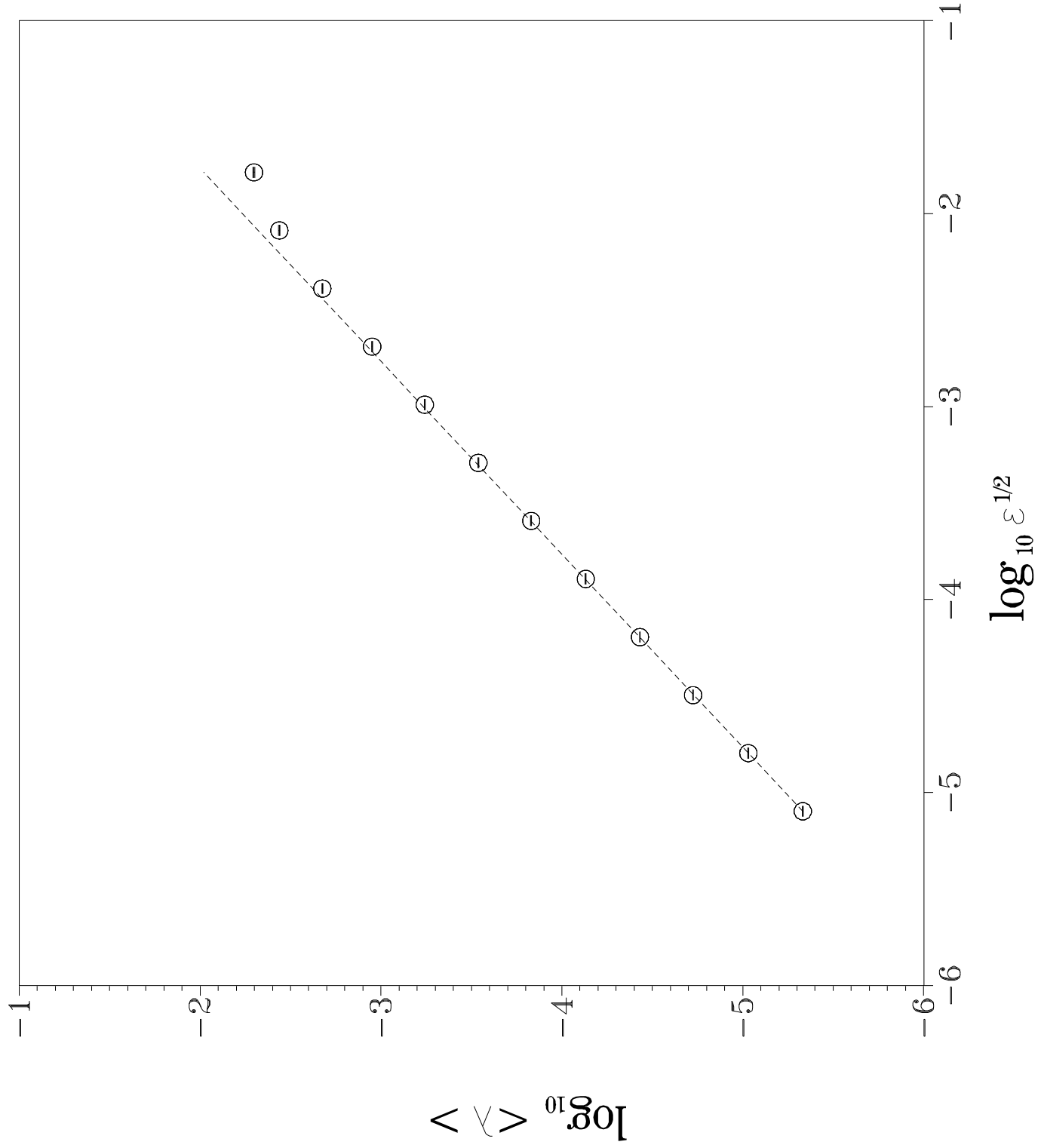


Fig. 1

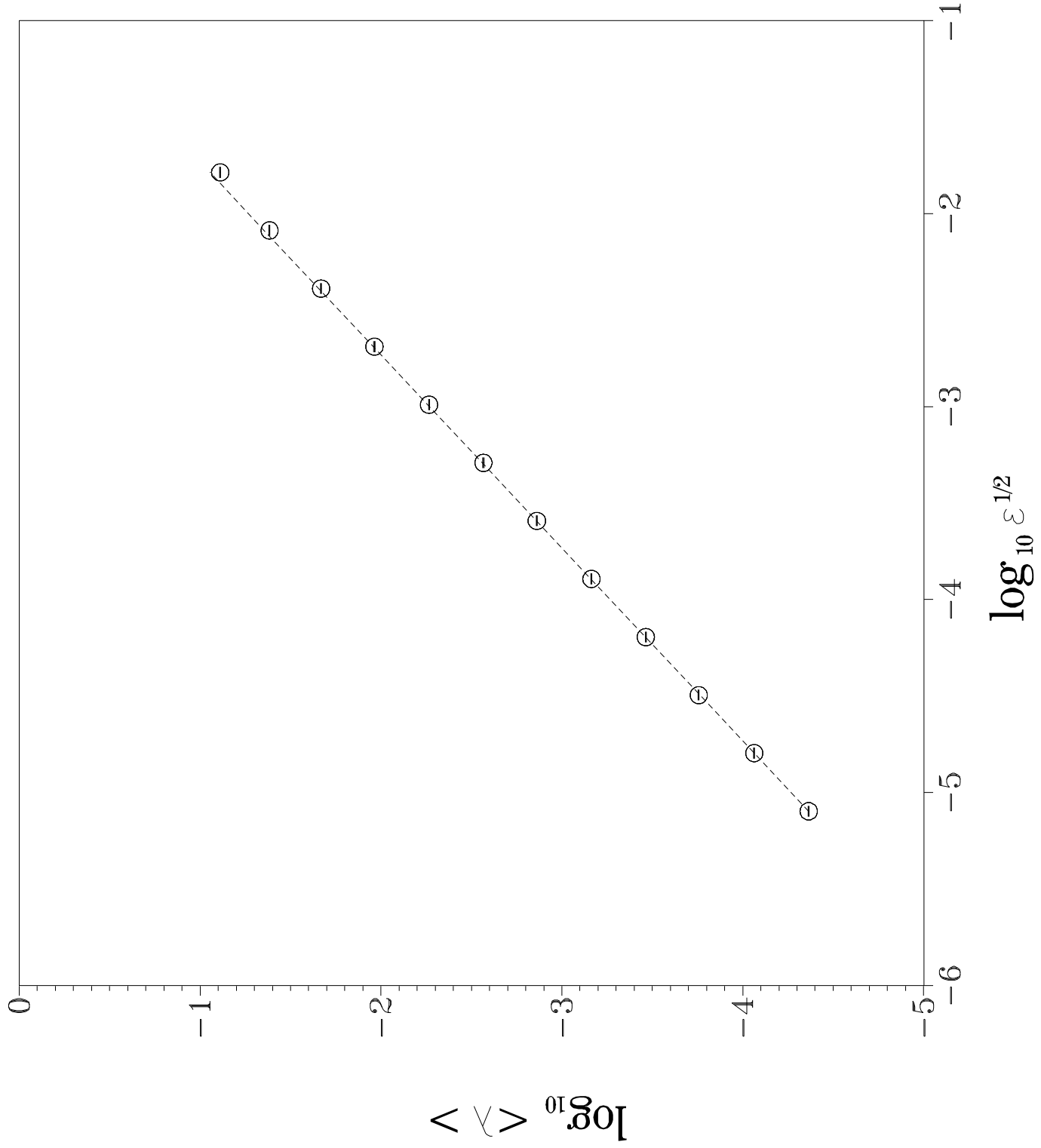
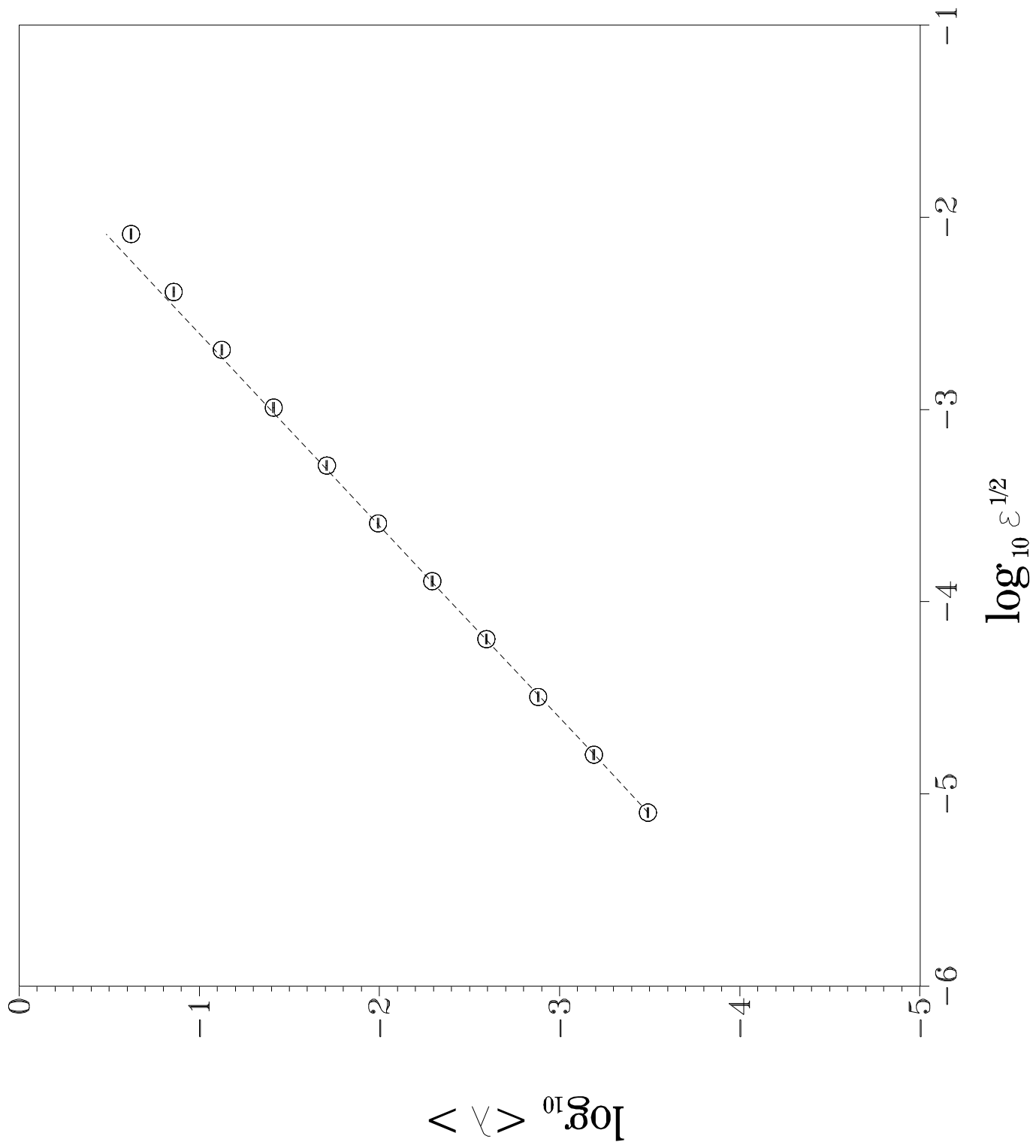


Fig. 2

Fig. 3



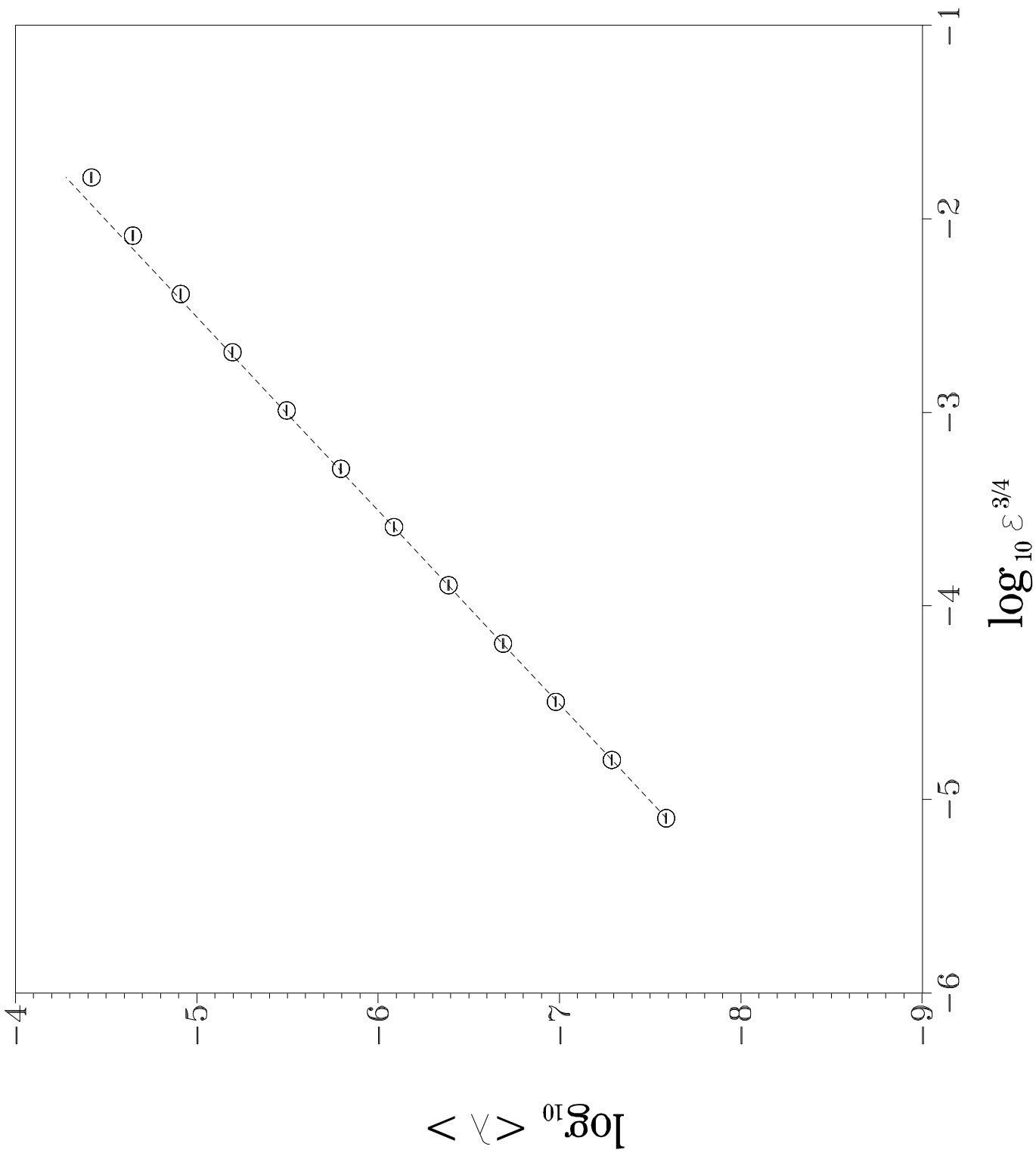
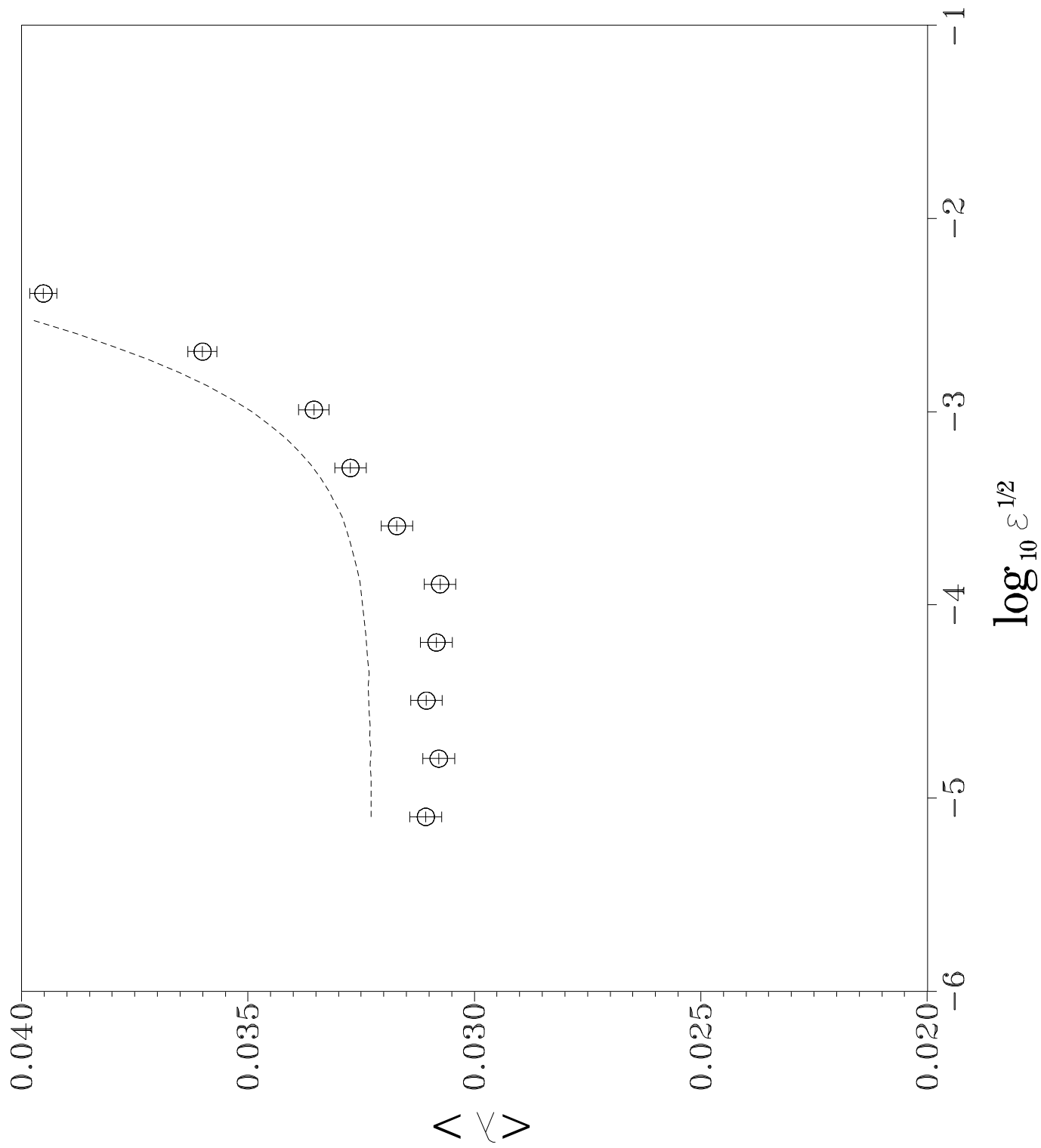


Fig. 4

Fig. 5



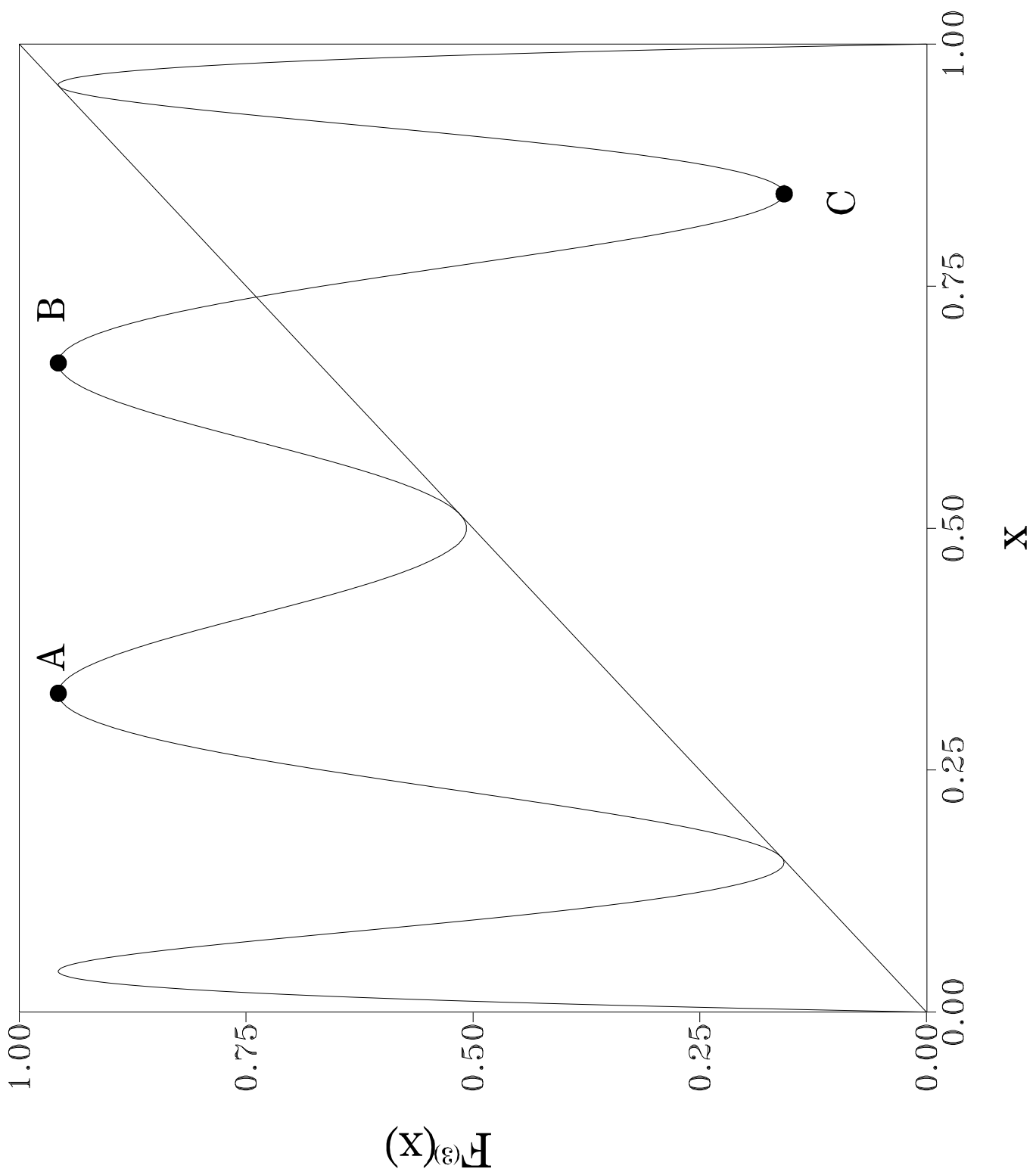


Fig. 6

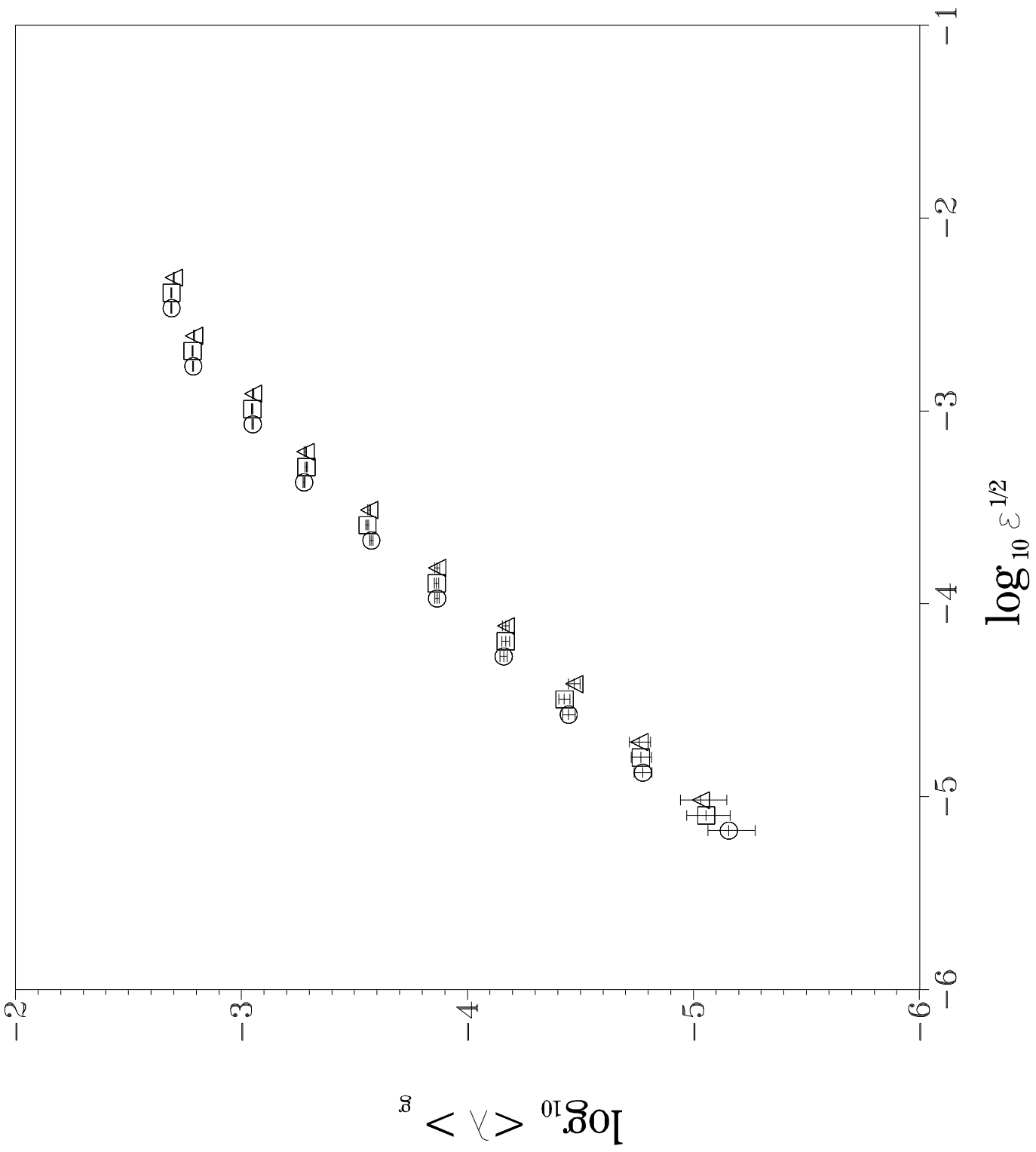


Fig. 7

Fig. 8

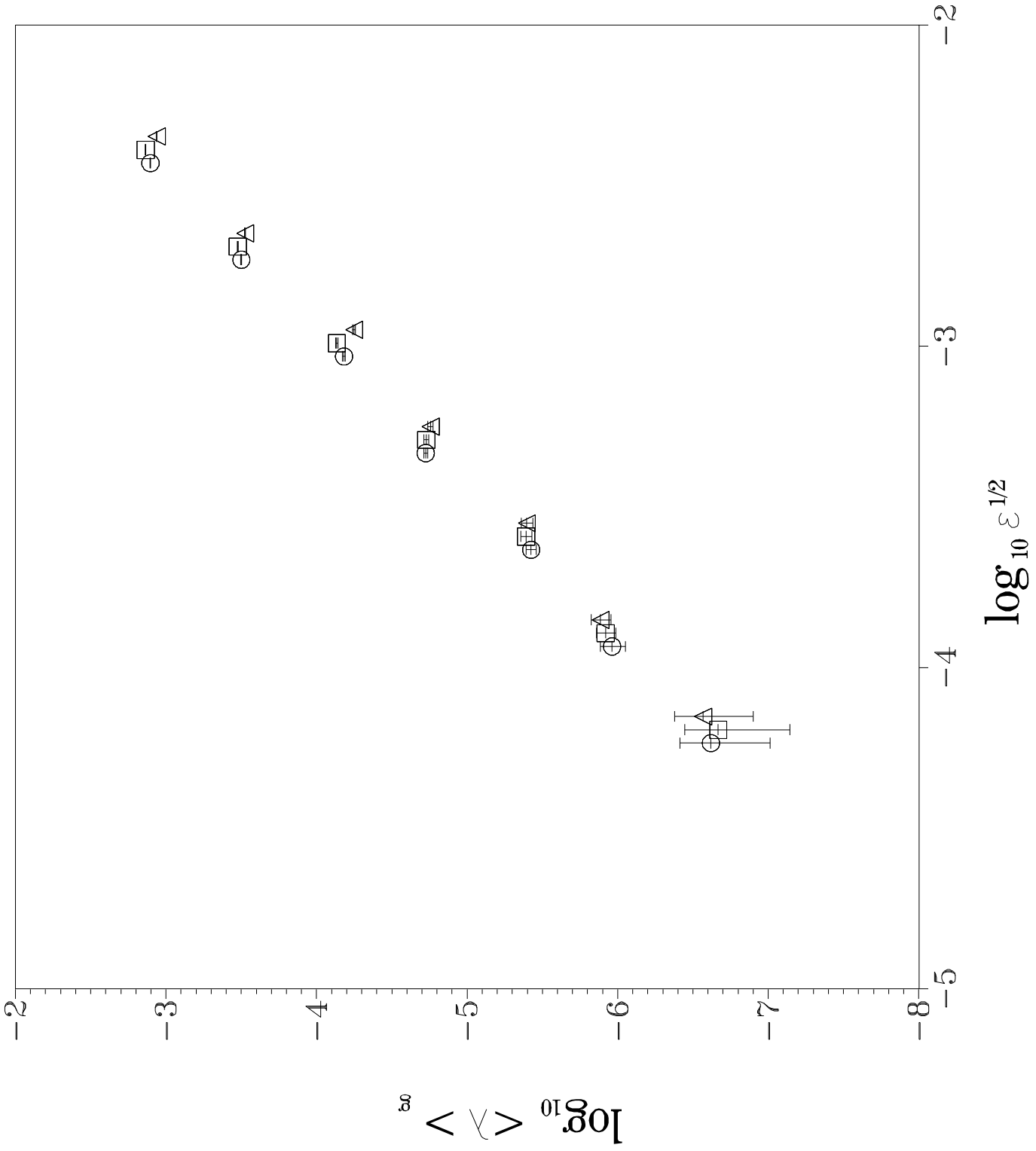


Fig. 9

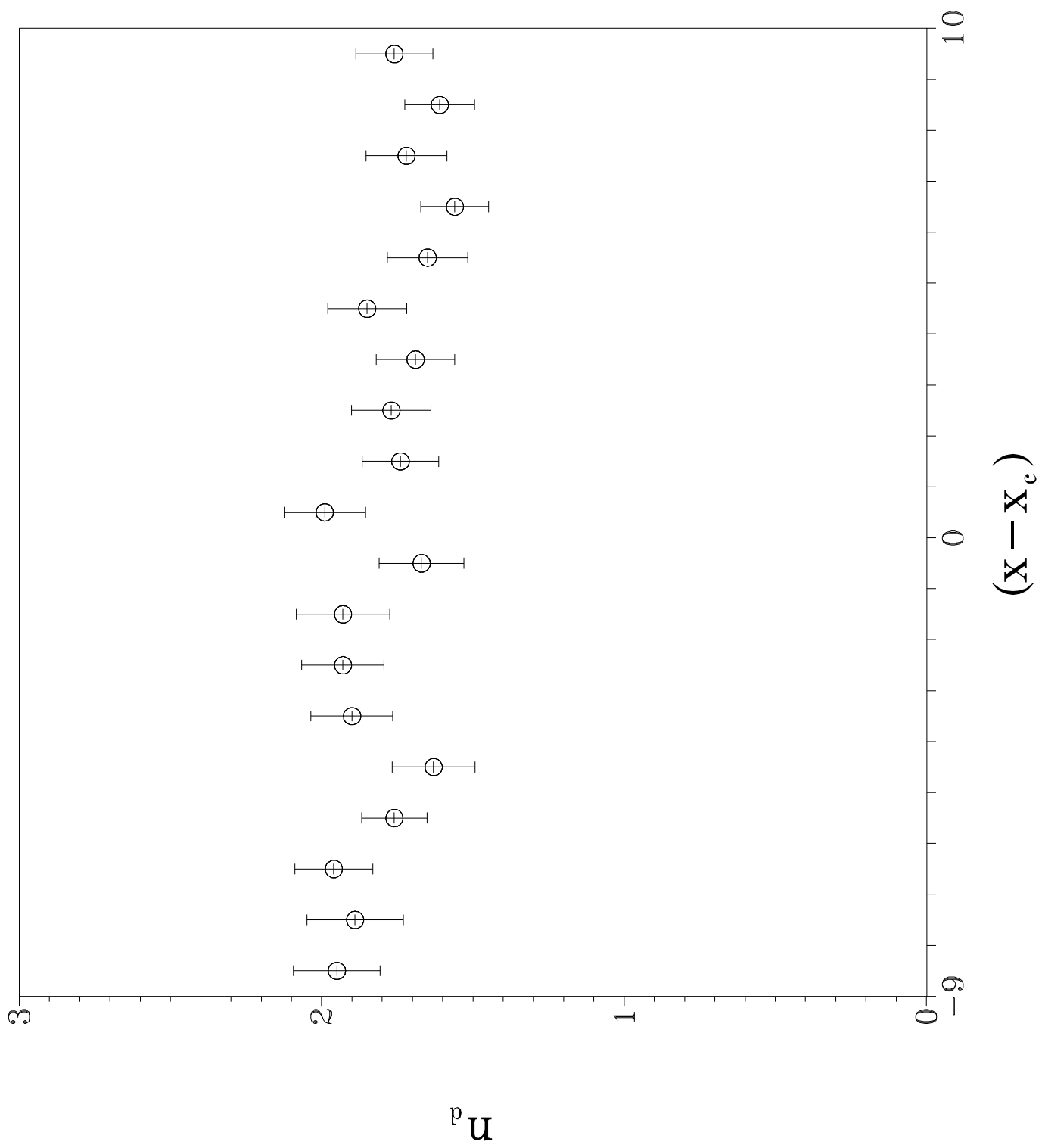


Fig. 10

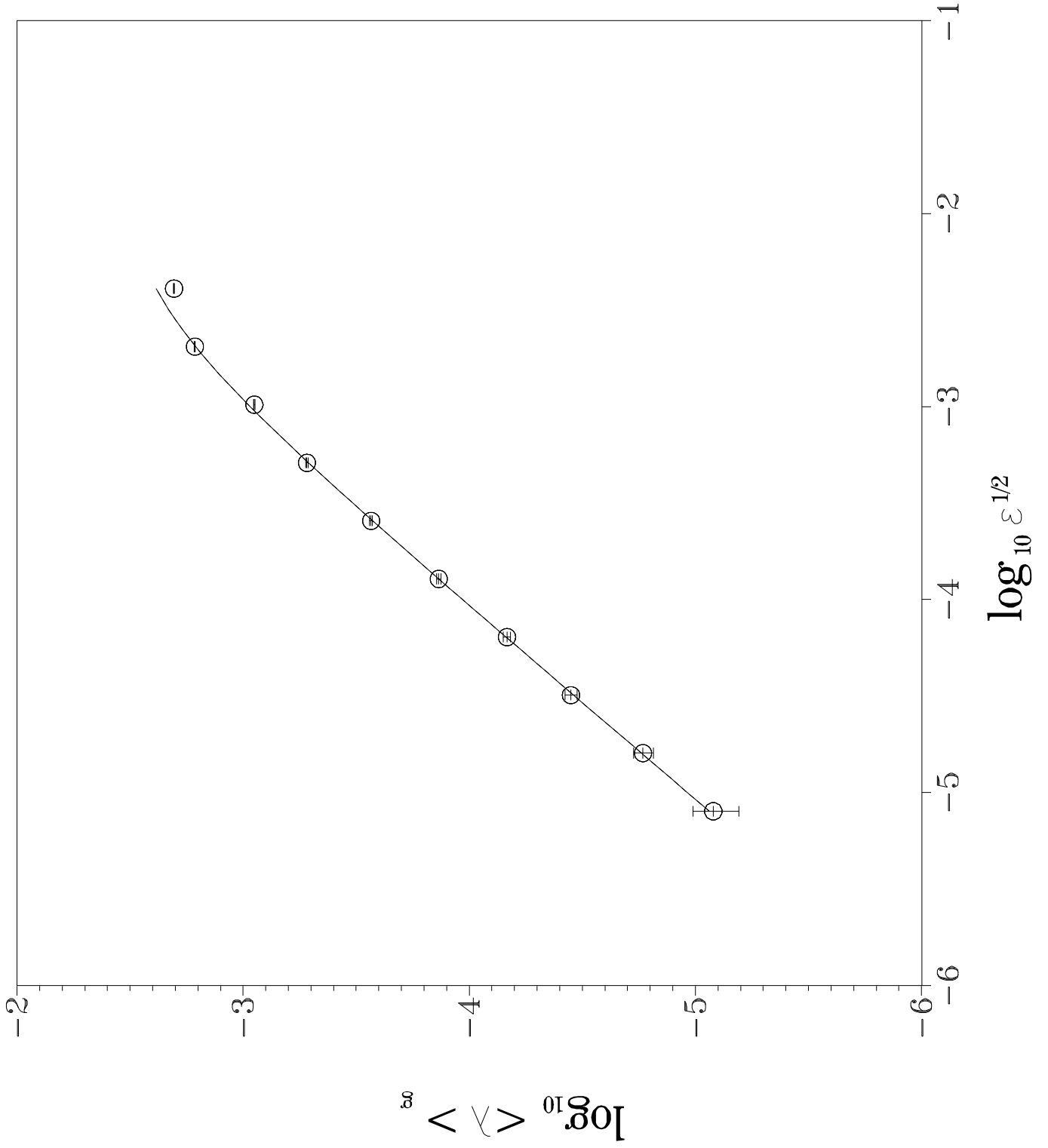


Fig. 11

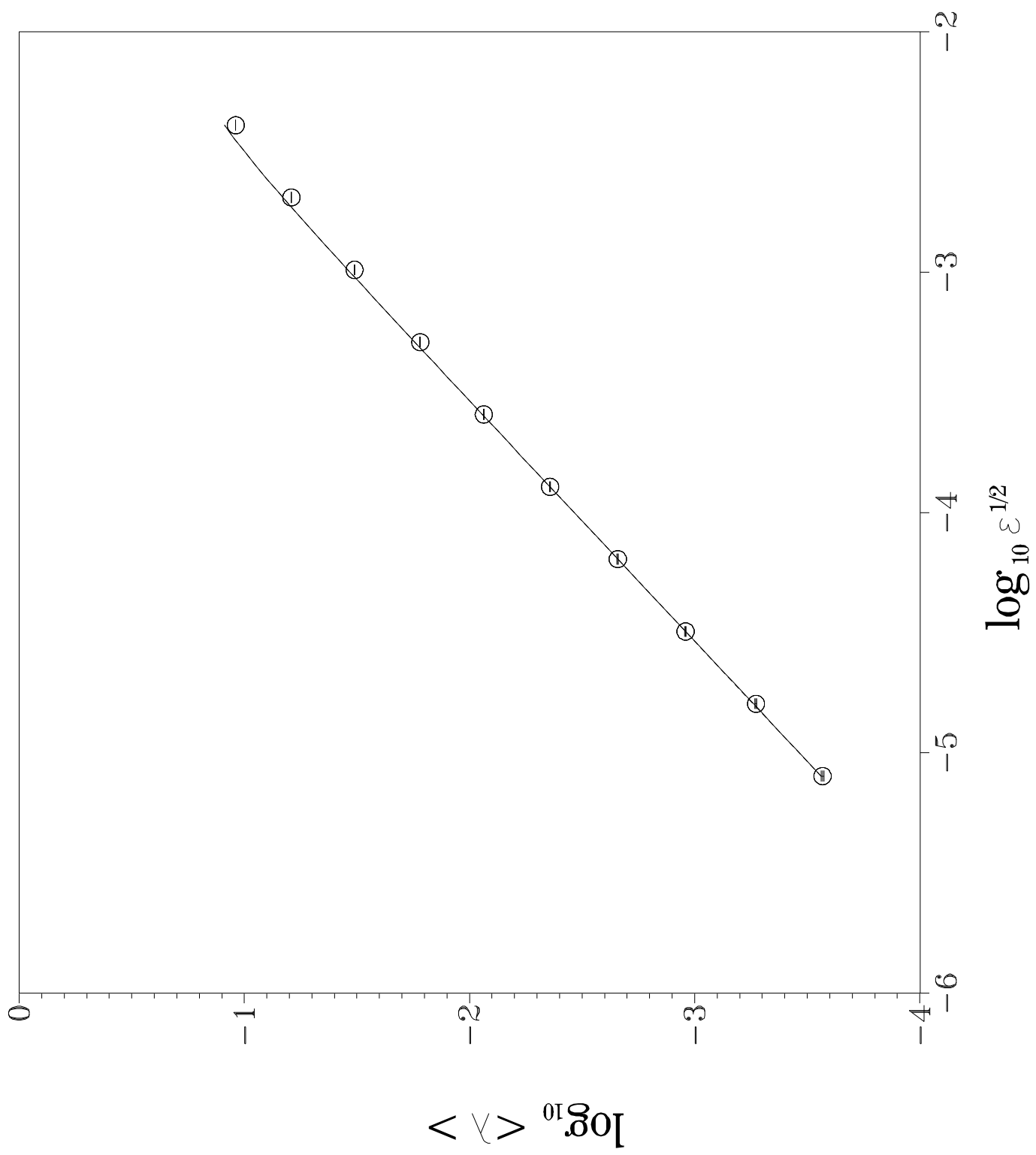


Fig. 12

